

International Journal of Modern Physics A  
 © World Scientific Publishing Company

## Measurement of heavy-flavor electron production in Au+Au collisions at $\sqrt{s_{NN}} = 54.4$ GeV at STAR

Veronika Prozorova (for the STAR Collaboration)

*Faculty of Nuclear Sciences and Physical Engineering, Czech Technical University in Prague,  
 Brehova 7  
 Prague, 115 19, Czech Republic  
 veronika.prozorova@cvut.cz*

Received Day Month 2024

Revised Day Month Year

1 Studying heavy-flavor production in heavy-ion collisions (HIC) can enhance our com-  
 2 prehension of parton interactions with the Quark-Gluon Plasma (QGP) created in these  
 3 collisions. Due to their significant mass, heavy quarks (charm and bottom) are mainly  
 4 generated during the initial phase of high-energy HIC when hard scatterings are preva-  
 5 lent, and experience the entire evolution of the QGP. One way to study heavy quarks  
 6 is through the measurement of electrons from heavy flavor hadron decay, Heavy Flavor  
 7 Electrons (HFE). In this contribution, we present analysis of HFE at low transverse mo-  
 8 mentum ( $p_T$ ) in Au+Au collisions at  $\sqrt{s_{NN}} = 54.4$  GeV using data taken in 2017 by  
 9 the STAR experiment. The strong HFE suppression was already observed in the central  
 10 Au+Au collisions at  $\sqrt{s_{NN}} = 200$  GeV. Measuring heavy-flavor quark nuclear modifica-  
 11 tion factors below the RHIC top energy offers new insights on the the in-medium energy  
 12 loss, especially the collisional energy loss which is dominant at low  $p_T$ .

13 *Keywords:* Quark-Gluon Plasma; Heavy-flavor; STAR

14 *PACS numbers:*

### 15 1. Introduction

16 Quantum Chromodynamics (QCD) is the underlying theory of strong interaction.  
 17 At a very high temperature or and low baryon chemical potential, models inspired  
 18 by QCD predict a phase transition from the hadron gas to a deconfined medium  
 19 called Quark-Gluon Plasma (QGP). This state of matter existing under extreme  
 20 conditions of high temperature and density is of fundamental interest. By colliding  
 21 heavy ions at ultra-relativistic energies, it is possible to explore the QCD phase  
 22 diagram and properties of the QGP.

23 One of the tools to study QGP properties is to use heavy quarks. Given that  
 24 the masses of heavy quarks are considerably larger than the QCD scale parameter,  
 25  $\Lambda_{QCD}$ , and the QGP temperature, they are dominantly produced in the initial hard  
 26 scatterings and thus participate in whole medium evolution. Moreover, such partonic  
 27 processes can be calculated by perturbative QCD. These factors make heavy quarks

2 Veronika Prozorova

28 the ideal probes of QGP. With heavy quarks one can study the nature of energy  
 29 loss (collisional or radiative) by using nuclear modification factor.

30 One of the proxies for measuring heavy quarks is to use heavy-flavor electrons  
 31 (HFE), electrons coming from the semileptonic decays of open heavy-flavor hadrons  
 32 ( $D$  and  $B$ ). The relative contributions of  $D$  and  $B$  hadron decays depend on electron  
 33  $p_T$ : at low momenta  $D$  mesons are dominant. The branching ratio of semileptonic  
 34 decays is higher than that of hadronic decays, which makes HFE a valuable tool for  
 35 studying heavy quarks production.

36 Fig. 1 depicts recent STAR results for the nuclear modification factor,  $R_{AA}$ , as  
 37 a function of  $p_T$  for various centrality classes in Au+Au collisions at a center-of-  
 38 mass energy of  $\sqrt{s_{NN}} = 200$  GeV.<sup>1</sup> A suppression by a factor of two is observed  
 39 in central collisions indicating a significant energy loss of heavy quarks in QGP.  
 40 A larger suppression is observed in central collisions than in peripheral collisions,  
 41 which is consistent with expectations. It is now of interest to examine the energy  
 42 loss at lower energies, such as 54.4 GeV, following up on a recent STAR publication  
 of elliptic flow of HFE at this energy.<sup>2</sup>

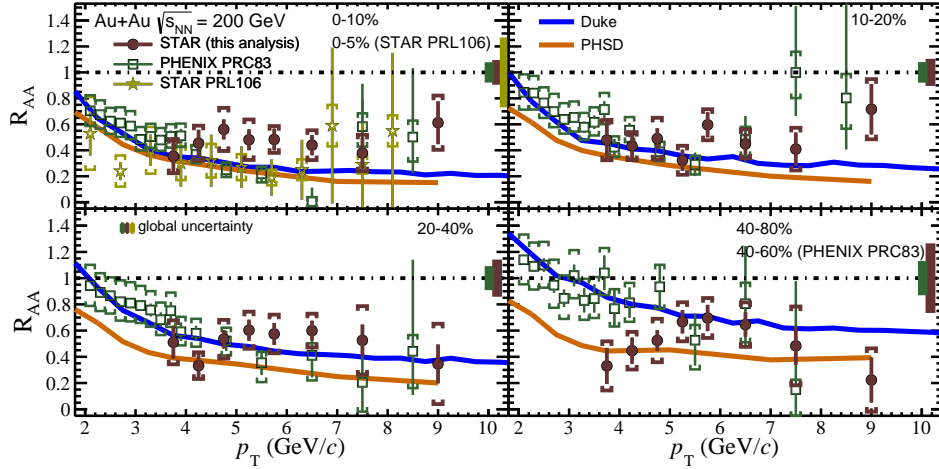


Fig. 1. HFE  $R_{AA}$  (full circles) as a function of  $p_T$  in different centrality intervals in Au+Au collisions at  $\sqrt{s_{NN}} = 200$  GeV<sup>1</sup> compared with STAR<sup>3</sup> (stars) and PHENIX<sup>4</sup> (empty squares) published results and Duke (blue line) and PHSD (orange line) model calculations.

43

## 44 2. Analysis

45 The experimentally identified electrons, named inclusive electrons  $e^{\text{incl}}$ , include the  
 46 following components:

- 47 (i) Photonic electrons,  $e^{\text{PE}}$ ;  
 48 (a) Dalitz decays:  $\eta \rightarrow \gamma e^+ e^-$ ,  $\pi^0 \rightarrow \gamma e^+ e^-$ ,

- 49 (b) Gamma conversion:  $\gamma \rightarrow e^+e^-$ ,  $\eta \rightarrow \gamma\gamma$ ,  $\pi^0 \rightarrow \gamma\gamma$ .  
 50 (ii) Hadron-decayed electrons,  $e^{\text{HDE}}$ , from  $\rho$ ,  $\omega$ ,  $\phi$ ,  $J/\psi$ , Drell-Yan and  $K_{e3}$ .

51 The HFE yield can be then calculated as:

$$N^{\text{HFE}} = \frac{N^{\text{incl}} \cdot \text{purity} - N^{\text{PE}}/\varepsilon^{\text{PE}}}{\varepsilon^{\text{total}}} - N^{\text{HDE}}, \quad (1)$$

52 where  $N^{\text{incl}}$  is the inclusive electron yield,  $N^{\text{PE}}$  is the photonic electron yield, *purity*  
 53 is the purity of the inclusive electrons,  $\varepsilon^{\text{PE}}$  is the photonic electron identification  
 54 efficiency,  $\varepsilon^{\text{total}}$  is the total efficiency of electron identification and reconstruction,  
 55  $N^{\text{HDE}}$  are hadron-decayed electrons.<sup>2</sup> The fraction in Eq. 1 is also referred to as  
 56 the non-photonic electron yield. The photonic electron identification efficiency is  
 57 calculated by propagating  $\gamma$  conversions,  $\pi^0$  and  $\eta$  decays through the GEANT  
 58 simulation of the STAR detector<sup>2</sup> before embedding them into real events.

### 59 2.1. Inclusive electron identification

60 Inclusive electrons are identified using information from the Time Projection Cham-  
 61 ber (TPC),<sup>5</sup> Time Of Flight (TOF),<sup>6</sup> and Barrel ElectroMagnetic Calorimeter  
 62 (BEMC).<sup>7</sup> The TPC is employed to reconstruct the particle momentum and identify  
 63 it using the energy loss,  $dE/dx$ , and momenta,  $\mathbf{p}$ . For this we use an  $n\sigma_x$  parameter  
 64 which is derived from the particle energy loss according to the formula:

$$n\sigma_e = \frac{1}{R} \ln \frac{\langle dE/dx \rangle_{\text{measured},x}}{\langle dE/dx \rangle_x}, \quad (2)$$

65 where  $R$  is STAR TPC  $\ln dE/dx$  resolution. It relates the measured and the expected  
 66 energy loss in the TPC for a given particle species ( $x$ ). The  $n\sigma_e$  cut for the TPC  
 67 electron identification is following:

- 68 •  $p \leq 0.8 \text{ GeV}/c^2$ :  $(2.25p - 3) < n\sigma_e < 2$
- 69 •  $p > 0.8 \text{ GeV}/c^2$ :  $-1.2 < n\sigma_e < 2$

70 The TOF detector information is used to identify electrons in the low  $p_T$  region.  
 71 The  $1/\beta$  cut has been set to  $|1 - 1/\beta| < 0.025$  for all tracks with TOF information.  
 72 To get more statistics in the higher  $p_T$  region, for  $p_T \geq 1.5 \text{ GeV}/c^2$ , tracks without  
 73 TOF information were not excluded. The identification in the high  $p_T$  region,  $p_T >$   
 74  $1.25 \text{ GeV}/c^2$ , was done using the information from the BEMC. Since the mass of  
 75 the electron is almost equal to its energy, it is worth using the E/p ratio for electron  
 76 selection. The applied E/p cut is defined as  $0.6 < E/p < 1.6$ . Tracks that pass all  
 77 the aforementioned cuts are classified as inclusive electrons.

### 78 2.2. Photonic electron identification

79 Once the inclusive electron selection is done, one can identify photonic electrons. As  
 80 it is not possible to determine whether a single electron is a photonic electron or not,

4 *Veronika Prozorova*

81 it can be done statistically using the so-called photonic electron tagging method.<sup>8</sup>  
 82 Tagged electrons, which are identical to inclusive electrons, are paired with partner  
 83 electrons. In order to enhance the efficiency of photonic electron reconstruction,  
 84 partner electrons have more loose selection criteria, which include track cuts and  
 85  $|\eta_{\sigma_e}| < 3$ . Then, the Distance of the Closest Approach (DCA) cut,  $|DCA| < 1$  cm,  
 86 and the invariant mass cut,  $M_{ee} < 0.1$  GeV/c, are applied to the pair. In the event  
 87 that the pair comprises either an electron or a positron, it is designated as an unlike-  
 88 sign (UL) pair, which is indicative of real PE. In the event that the pair comprises  
 89 either two electrons or two positrons, it is designated as a like-sign (LS) pair, which  
 90 describes the background. The background is calculated as a geometrical mean of  
 91 LS pairs:

$$N^{\text{LS}} = 2\sqrt{N^{e^+e^+}N^{e^-e^-}} \quad (3)$$

92 and is subsequently subtracted from the UL to obtain the photonic electron yield.  
 93 Fig.2 shows the invariant mass selection of photonic electrons in central (left) and  
 94 peripheral (right) collisions in one of the measured  $p_T$  intervals. Red circles and black  
 95 squares show the LS and UL pairs, respectively. The UL signal with background  
 96 subtracted is shown by blue triangles. Purple dashed line represents used invariant  
 97 mass cut.

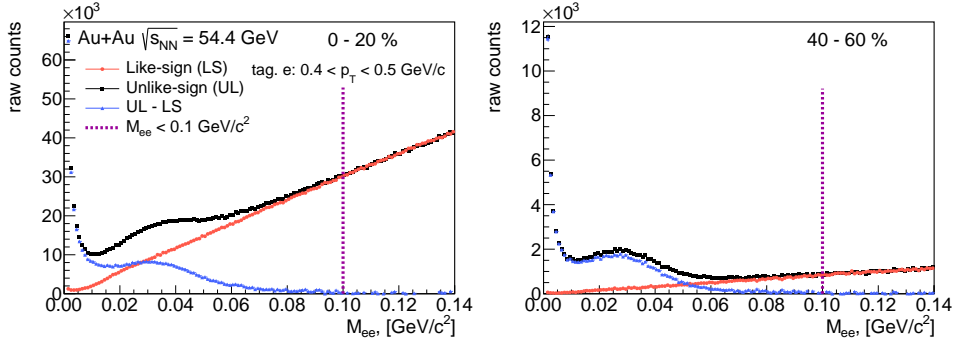


Fig. 2. Invariant mass selection of photonic electrons in central (left) and peripheral (right) collisions.

### 98 **2.3. Purity and $n\sigma_e$ cut efficiency**

99 It is important to estimate the purity of inclusive electrons. First, the pure hadron  
 100 and photonic electron samples are identified using the cuts listed in the Table 1.  
 101 Afterwards, pure samples are fitted with the Gaussian function in different  $p_T$  in-  
 102 tervals, and the mean and sigma values extracted from the fits for each  $p_T$  interval.  
 103 Next, these values are used for fitting the  $n\sigma_e$  distributions after applying TOF and  
 104 BEMC electron identification with a multi-Gaussian function. An example of such  
 105 fits for different  $p_T$  intervals in 0 - 20 % centrality is shown in Fig. 3. Different colors

106 correspond to different particle species, while the dashed light-blue line represents  
 107 the total fit. As it can be seen, there are momentum regions where the electron  
 108  $dE/dx$  overlaps with that of other hadrons: kaons (Fig. 3 left), protons and merged  
 109 pions (Fig. 3 right). These regions will have lower purity.

Table 1. Selection cuts for pure hadron and electron samples.

Particle	Mass cut, ( $\text{GeV}/c^2$ )	$n\sigma_e$ cut
proton	$ m_p^2 - 0.879  < 0.02$	$ n\sigma_p  < 4$
kaon	$ m_K^2 - 0.243  > 0.05$	$ n\sigma_K  < 4$
merged $\pi$	$ m_{\text{merged}\pi}^2 - 0.019  > 0.03$	$ n\sigma_{\text{merged}\pi}  < 5$
electron	$m_e^2 < 0.04$	$ n\sigma_e  < 3$

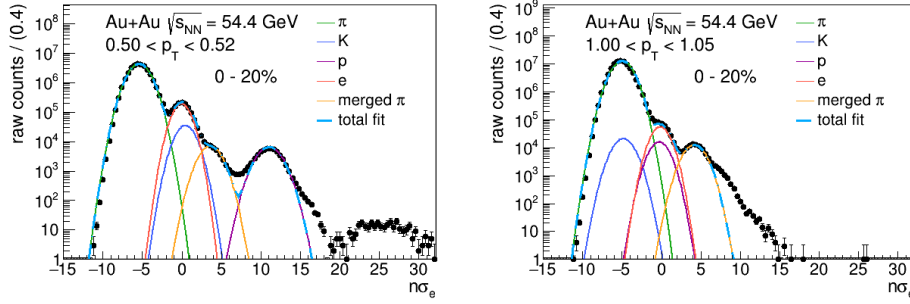


Fig. 3. An example of  $n\sigma_e$  fits for 0 - 20 % centrality.

### 110 3. Results

111 In this section some components needed for the HFE yield calculation (Eq. 1) are  
 112 presented. The uncorrected raw inclusive and photonic electron yields for different  
 113 centralities are shown in Fig. 4. The bumped structure is a consequence of the  
 114 utilization of BEMC, TOF, and TPC for electron identification, with the BEMC  
 115 energy over momentum ratio employed from  $p_T > 1.25 \text{ GeV}/c$ .

116 The total efficiency of electron identification and reconstruction consists of the  
 117 following components: TPC tracking, TOF and BEMC matching efficiencies,  $1/\beta$ ,  
 118  $E/p$  and  $n\sigma_e$  cut efficiencies. The efficiencies for TPC tracking, BEMC matching,  
 119 and the  $E/p$  cut are obtained from STAR detector simulations. In contrast, the  
 120 other efficiencies are calculated using a pure electron sample in the data. Fig. 5  
 121 depicts the  $1/\beta$  (left) efficiency which is approximately 0.98 throughout the whole  
 122  $p_T$  range. The BEMC matching and  $E/p$  cut efficiencies are shown in Fig. 5 (right)  
 123 and are approximately 85% for  $p_T > 1.25 \text{ GeV}/c$ .

6 Veronika Prozorova

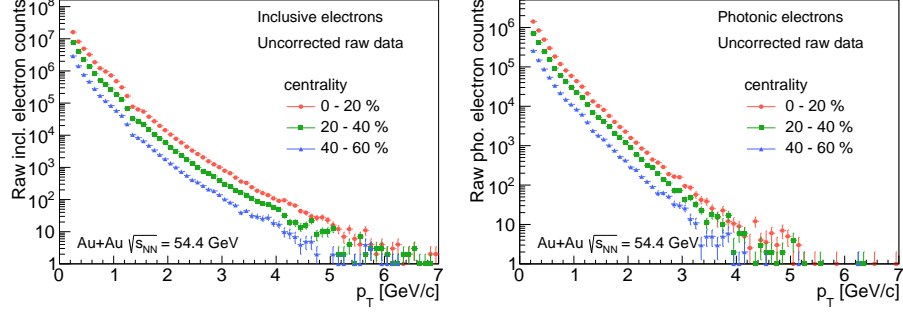
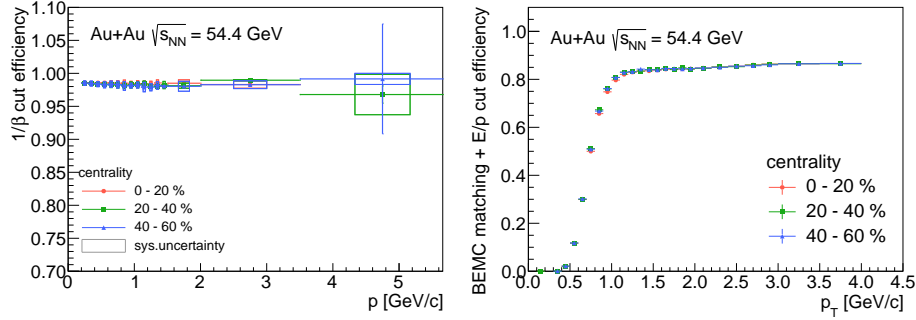


Fig. 4. Raw inclusive (left) and photonic (right) electron yields for different centrality ranges.


 Fig. 5.  $1/\beta$  (left) and BEMC matching +  $E/p$  cut (right) efficiencies for different centralities.

#### 124 4. Conclusion and outlook

125 These proceedings present an ongoing analysis of the heavy-flavor electron produc-  
 126 tion measurement in Au+Au collisions at 54.4 GeV/c. The various components of  
 127 Eq. 1, including the raw inclusive and photonic electron yields, the  $1/\beta$  cut effi-  
 128 ciency, the BEMC matching efficiency, and the  $E/p$  cut efficiency, were presented.  
 129 The subsequent step is to calculate the non-photonic electron yield and subtract the  
 130 hadron contribution in accordance with Eq. 1. It is planned to measure central-to-  
 131 peripheral nuclear modification factors as functions of  $p_T$ . This will provide further  
 132 insight into the interaction of charm quarks with the QGP medium and, thereby  
 133 complementing the existing results at  $\sqrt{s_{NN}} = 200$  GeV and the recent HFE  $v_2$   
 134 measurement at  $\sqrt{s_{NN}} = 54.4$  GeV.

#### 135 Acknowledgments

136 This work was supported by the Grant Agency of the Czech Technical University  
 137 in Prague under grant No. SGS22/174/OHK4/3T/14, and by the Ministry of Edu-  
 138 cation, Youth, and Sports of the Czech Republic through the project LM2023034,  
 139 Brookhaven National Laboratory - the participation of the Czech Republic. Ad-

ditional support was provided by the Martina Roeselová Memorial Fellowship,  
awarded by the IOCB TECH Foundation in 2024.

## References

1. M.I. Abdulhamid et al. (STAR Collaboration), *JHEP* **06** (2023) 176.
2. M.I. Abdulhamid et al. (STAR Collaboration), *Phys. Lett. B* **844** (2023) 138071.
3. STAR collaboration, *Phys. Rev. D* **83** (2011) 052006.
4. PHENIX collaboration, *Phys. Rev. Lett.* **97** (2006) 252002.
5. M. Anderson et.al (STAR Collaboration), *Nucl. Instrum. Meth. A* **499** (2003) 659-678.
6. W.J. Llope, *Nucl. Instrum. Meth. B* **241** (2005) 306-310.
7. M. Beddo et al (STAR Collaboration), *Nucl. Instrum. Meth. A* **499** (2003) 725-739.
8. H. Agakishiev et al. (STAR Collaboration), *Phys. Rev. D* **83** (2011) 052006.